Evolution of chemical and mechanical properties in two-photon polymerized materials during pyrolysis

Aofei Mao, Hibiki Mitsuboshi, Maxime Trochon, Xiang Zhang, Lanh Trinh, Sedighe Keynia, Peixun Fan, Nada Kraiem, Xi Huang, Nan Li, et al.

Evolution of chemical and mechanical properties in two-photon polymerized materials during pyrolysis

Aofei Mao[1#]. Hibiki Mitsuboshi[2#]. Maxime Trochon[3#], Xiang Zhang[4], Lanh Trinh[4], Sedighe Keynia[4], Peixun Fan[1], Nada Kraiem[1,5], Xi Huang[1], Nan Li[1], Peizi Li[1], Zhipeng Wu[1], Wanting Sun[1], Bai Cui[4], Jean-Francois Silvain[1,5], Masanori Hara[2], Masamichi Yoshimura[2], Kenneth L. Marshall[6], Mitchell Anthamatten[7], Yongfeng Lu[1*]

[1]Department of Electrical and Computer Engineering, University of Nebraska, Lincoln, NE 68588, USA.

[2]Graduate School of Engineering, Toyota Technological Institute, Nagoya, Aichi, 468-8511, Japan.

[3]Graduate School of Engineering, Bordeaux Institute of Technology (Bordeaux INP), Bordeaux, France.

[4]Department of Mechanical and Materials Engineering, University of Nebraska, Lincoln, NE 68588, USA.

[5]CNRS, University of Bordeaux, Bordeaux I.N.P., ICMCB, UMR 5026, F-33608 Pessac, France.

[6]Laboratory for Laser Energetics, University of Rochester, Rochester, NY 14627, USA.

[7]Department of Chemical Engineering, University of Rochester, Rochester, NY 14627, USA.

E-mail: ylu2@unl.edu

Abstract

Fabrication of three-dimensional (3D) carbon-based structures at micro/nanoscale, mainly by pyrolysis of photocured resins, has recently drawn attention in battery development, material engineering, and catalysts. Upon pyrolysis, photocured 3D polymer structures undergo thermal decomposition and eventually carbonize while maintaining their 3D features. Herein, we systemically investigate the physical and chemical reactions that occur during the pyrolysis of

[#]Authors contributed equally to this paper.

methacrylate-based resin structures, yielding fundamental knowledge and an improved understanding of the pyrolysis processes. Based on our results, the pyrolysis process can be divided into three stages: monomer evaporation, chemical decomposition, and carbonization, in which the volume shrinkage mainly occurs in the first and third stages. The three stages have different effects on the mechanical properties of the pyrolyzed structures, with monomer evaporation and carbonization enhancing the Young's modulus while decomposition reduces the Young's modulus. Additionally, the surface smoothness of the photocured structures can be improved during pyrolysis due to the shrinkage of the polymer resins, which provides a potential approach to generating ultrasmooth carbon surfaces.

Keywords: Two-photon polymerization, pyrolysis, pyrolyzed carbon, shrinkage, chemical composition, Young's modulus, Raman spectroscopy

1. Introduction

Direct laser writing by two-photon polymerization (2PP) has shown its capability in shaping polymers with complex 3D geometry and feature sizes down to 100 nm.[1,2] This method is a proven, powerful tool for fabrication of spherical inertial confinement fusion targets [3,4], 4D printing [5,6], micro-optics [7,8], and carbon microelectromechanical system (C-MEMS).[9,10] However, the material selection for 2PP is generally limited to polymers, which sometimes lack electrical conductivity and mechanical stability.[11] To address these limitations, nanotubes [12], noble metals [13,14], SiO_2 [15], and magnetic materials [16,17] have been successfully integrated with 2PP to extend the properties of two-photon polymerized materials beyond the normal ranges of polymers. Besides material adaption, post-processing of 2PP structures, including electroplating [18], lithiation [19], atomic layer deposition [20], plasma etching [21], and pyrolysis [22] also possess great potentials. Among all these techniques,

[#]Authors contributed equally to this paper.

pyrolysis of the 3D-printed polymers simultaneously improves mechanical robustness, print resolution, and enables thermal and electrical conductivity.

Briefly, pyrolysis is a process by which polymer chains undergo thermal degradation into smaller volatile molecules, monomers, or a mixture of organic compounds, which generally includes evaporation, depolymerization, random chain scission, and side-group scission. Along with the chain scission and material loss, the precursors transform into either glassy carbon or ceramic depending on the materials. [23] Pyrolysis of polymer structures can result in valuable materials including ultra-strong carbon lattices [22,24], carbon electrodes with high electrical capacitance [25], and other functional devices such as neurotransmitter sensors, atomic force microscopy tips, photonic crystals, and so on. [26–31] To investigate the pyrolysis process, various studies have focused on the effect of maximum temperature, ramp speed, and environment on the mechanical properties and resistivities of pyrolyzed polymers. However, the impact of pyrolysis on composition as well as the mechanical and physical properties of two-photon polymerized resins remains unclear.

To address the knowledge gap in pyrolysis of 2PP resins, we systematically conducted pyrolysis of Nanoscribe's IP-Q as a model methacrylate-based resin, and we analyzed the resulting properties. Specifically, we used 2PP to 3D-print foam structures and subjected them to pyrolysis under different conditions. Raman spectroscopy, X-ray photoelectron spectroscopy (XPS), nanoindentation, transmission electron microscopy (TEM), and scanning electron microscopy (SEM) were performed on the pyrolyzed material to establish new relationships between composition and the resulting mechanical and physical properties.

[#]Authors contributed equally to this paper.

2. Materials and methods.

Materials. The photoresist used in this study is IP-Q (Nanoscribe GmbH) which consists of a methacrylate monomer (7,7,9(or7,9,9)-trimethyl-4,13-dioxo-3,14-dioxa-5,12-diazahexadecane-1,16 diyl bismethacrylate, CAS NO. 72869-86-4), inhibitor (2,6-di-tert-4-butylhydroxytoluene, CAS NO. 128-37-0) and photoinitiators. During the experiments, a femtosecond (fs) laser was focused into the resin pool to induce two-photon absorption. The focused laser beam decomposes initiators into free radicals by two-photon photolysis. Formed radicals consume the C=C bonds of methacrylate-containing monomers to create carbon-carbon single bonds, leading to highly crosslinked/solidified polymer networks, as shown in Figures 1a&d. By scanning the laser spot in a 3D trajectory, complex 3D polymer structures could be

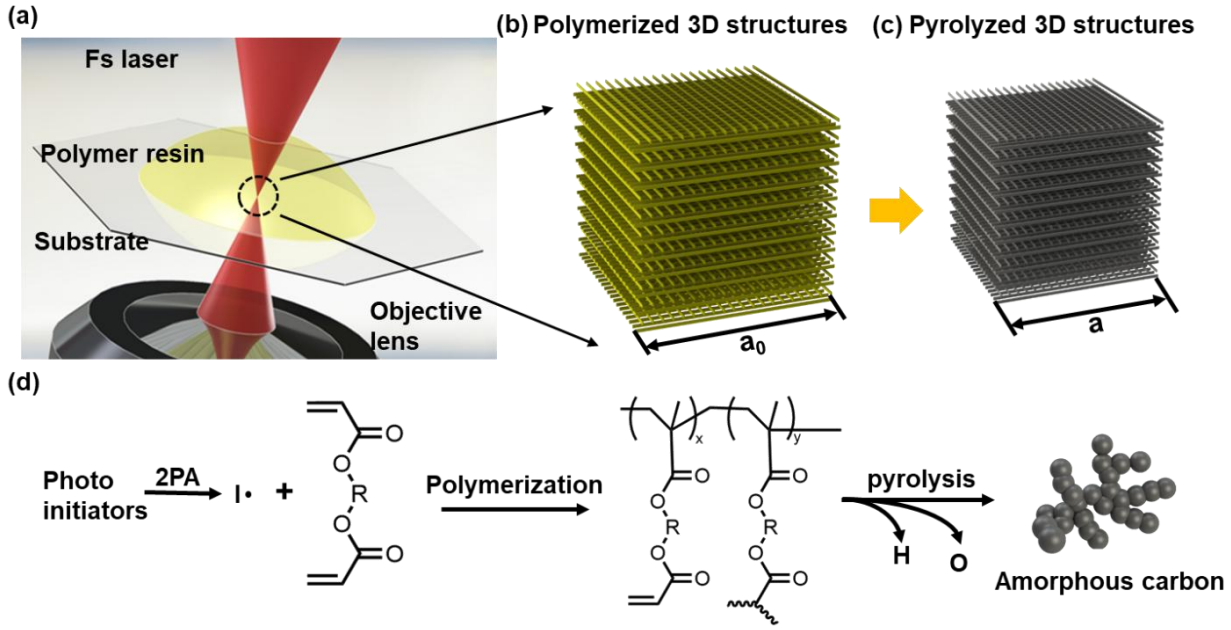

printed and subsequently transformed into 3D carbon structures upon pyrolysis, as shown in Figures 1b-c.

Figure 1. A schematic graph of the 2PP and pyrolysis processes. (a&b) 2PP and the as-printed foam structure. (c) 3D carbon structure formed after pyrolysis. (d) the elements and chemical structures depicting material changes during 2PP and pyrolysis.

[#]Authors contributed equally to this paper.

Two-photon polymerization: All samples used in this study, including the foam structures and solid cubes for nanoindentation, were fabricated using a commercial 2PP system (Photonic Professional GT from Nanoscribe GmbH). The fs laser was focused by a nanoscribe objective lens (10×, NA=0.3) and scanned by a computer-controlled galvo in the resins using the dip-in laser lithography configuration (DiLL). After printing, all samples were immersed in 50 mL of propylene glycol monomethyl ether acetate (PGMEA) (3M) for 1 hr to thoroughly dissolve the unreacted resin, followed by a rinse in 2-propanol (Sigma-Aldrich) for 20 min to remove residual PGMEA.

Pyrolysis: Pyrolysis was carried out in a 5-inch diameter tube furnace filled with argon gas (MTI corporation, GSL-1500x) at atmospheric pressure. Pyrolysis was conducted by ramping up to a maximum temperature at a constant rate of 15 or 10 °C/min. The maximum temperature (referred to as "pyrolysis temperature") was maintained for a period of time ("pyrolysis time") before the furnace was allowed to cool down to room temperature by natural convection.

Surface roughness imaging: The surface profiles of the printed structures including shells were measured using a Keyence laser scanning microscope (VK-X200K) which works at a laser wavelength of 408 nm. A Nikon objective lens (CF Plan Apo, 150×, NA 0.95) was used to capture the fine details on the structural surfaces.

Raman spectroscopy: Raman spectra were acquired by a Renishaw inVia H18415 Raman microscope. The excitation source was an argon laser at a wavelength of 515 nm with a power of 50 mW. Light excitation and signal collection were carried out using a 50× objective lens with a numerical aperture of 0.50. Raman spectra were recorded with an accumulation time of 10 s. Obtained spectra were processed by OriginLab (for Raman data processing) to remove baselines

[#]Authors contributed equally to this paper.

and integrate peak areas.

Gas chromatography-mass spectrometry (GC-MS): GC-MS was conducted on a Hewlett-Packard 5988 GC-MS system with direct insertion probe sampling. The 3D-printed cylinders were inserted into a gold hollow probe sampling tip mounted on the direct insertion probe and inserted directly into the MS ion source through a vacuum interlock chamber. The probe is heated electrically from room temperature to 320 °C at a rate of 10 °C/min. Perfluorotributylamine (peak mass: 69, 219, 502) was used as a standard calibrant. The calibration measurement shows resulting peaks at 68.05, 218.85, and 502.05 respectively.

Scanning electron microscopy: A Hitachi S4700 field-emission scanning electron microscope (FE-SEM) was used to observe the shapes and morphologies of the 3D structures after pyrolysis. The dimensions of printed samples were estimated using ImageJ.

Nanoindentation: Nanoindentations were conducted using a Bruker Dimension Icon Atomic Force Microscope with a Tap300A indenter tip (spring constant: 40 N/m). Before the experiment, a tip-to-optic calibration was conducted to ensure that the spatial positioning on each sample was as accurate as possible. A 50× objective lens (long working distance) was used to observe the pyrolyzed structures.

X-Ray Photoelectron spectroscopy: X-ray photoelectron spectroscopy (XPS) was performed using a Thermo Fisher Scientific K-Alpha X-ray Photoelectron spectrometer. Samples were analyzed under a micro-focused Al K-α X-ray source operating at $2x10^{-7}$ mbar. Survey spectra were acquired with a pass energy of 200 eV to cover the elemental composition. High-resolution spectra of the individual elements were acquired with a pass energy of 50 eV. Spectra were processed using Originlab 2020.

Transmission electron microscopy: The pyrolyzed carbon material was extracted from

[#]Authors contributed equally to this paper.

the sample surface by a focused ion beam (FIB) using an FEI Helios 660 FIB and then thinned to electron transparency. Cross-sectional transmission electron microscopy and selective area electron diffraction (SAED) were conducted in a scanning transmission electron microscope (S/TEM, Tecnai Osiris, FEI) operating at 200 kV.

3. Results and discussion

3.1 Chemical compositional changes during pyrolysis.

It is believed that during pyrolysis, evaporation of volatile species and decomposition of the crosslinked polymer occur.[32] However, the exact physical process during pyrolysis remains unclear. Therefore, we conducted a series of experiments on how the pyrolysis temperature and pyrolysis time affect the pyrolysis process, as shown in Figure 2a. First, we collected the Raman spectra of the liquid resin and as-printed structures, as shown in Figure 2a. After polymerization, the peak intensity at C=C (1640 cm^{-1}) is significantly reduced due to the consumption of monomers. The degree of conversion (DoC) of 2PP was estimated by the following calculation:

$$\mathrm{DoC} = 1 - \left(\frac{\mathrm{A_{C=C}}/\mathrm{A_{C=O}}}{\mathrm{A'_{C=C}}/\mathrm{A'_{C=O}}}\right),$$

where $A_{C=C}$, $A_{C=O,}$ and $A'_{C=C}$, $A'_{C=O}$ are the integrated intensities of the corresponding peaks in the 2PP structures and the unpolymerized resin, respectively. The calculation shows that the DoC is only about 28.6%, and details of the calculation are provided in Figure S1. Therefore, after washing away the liquid resin, the printed structure is a mixture of monomers and polymers with a significant amount of unreacted methacrylate groups. After analyzing the composition of printed material, we conducted systematic experiments to investigate the effect of pyrolysis temperature and pyrolysis time on the composition of the two-photon polymerized material. For

[#]Authors contributed equally to this paper.

each sample we printed four foam structures by setting the laser power at 50 mW and scan speed at 10 mm/s. After development, samples were pyrolyzed at different temperatures (from 400 to 550 °C) with a constant ramp rate of 15 °C /min and held for 5 min at the pyrolysis temperature to study the effect of temperature on pyrolysis, as shown in the Raman spectra of Figures 2b. At 400 °C, the molecular vibrations of the skeletal -CH_3 group and C=O bonds are still obvious while the C=C bond vibration present on the monomer is greatly reduced, indicating that evaporation of monomer or further reaction of methacrylate groups occurs at the early stage of pyrolysis. Continuing to increase the pyrolysis temperature to 450 °C, no clear molecular vibration was detected in the Raman spectra, indicating that bond cleavage leading to thermal decomposition mainly occurs at this stage. When the temperature reached 500 °C, carbonization starts as the D (~1350 cm^{-1}) and G bands (~1575 cm^{-1}) attributed to sp^2 hybridization of carbon are clearly present in the Raman spectra. It is noteworthy that the carbonization temperature of IP-Q (500 °C) reported here is relatively lower than that of SU-8 (~600 °C), a widely-used resin.[33] The I_D/I_G ratio increased from 2.19 to 3.34 (as calculated in Figure S2) after the temperature reached 550 °C, and a similar trend (I_D/I_G ratio increases with the pyrolysis temperature) was been reported in prior studies.[34,35] This phenomenon could be explained as follows: as temperature increases, the heteroatoms in the printed material release, leading to an increase of disorder in the molecular structure which is responsible for the increase of the D band (disordered band).[34,36] To identify the volatiles and chain scission mechanism during pyrolysis, direct insertion probe quadrupole MS was also performed by ramping temperature at 10 °C /min up to 320 °C and showed mass loss with major peaks observed at m/z= 41, 69, 113, and 309, respectively, which are likely molecular fragments from the monomer repeat unit (as shown in Figure S3 and Table S1). The same fragments were observed when the unpolymerized

[#]Authors contributed equally to this paper.

IP-Q resin comprising of mostly monomer was heated to 320 °C under identical conditions, and this result also corroborates the idea that monomer evaporation from polymerized resin occurs at low temperatures (< 400 °C) as described earlier.

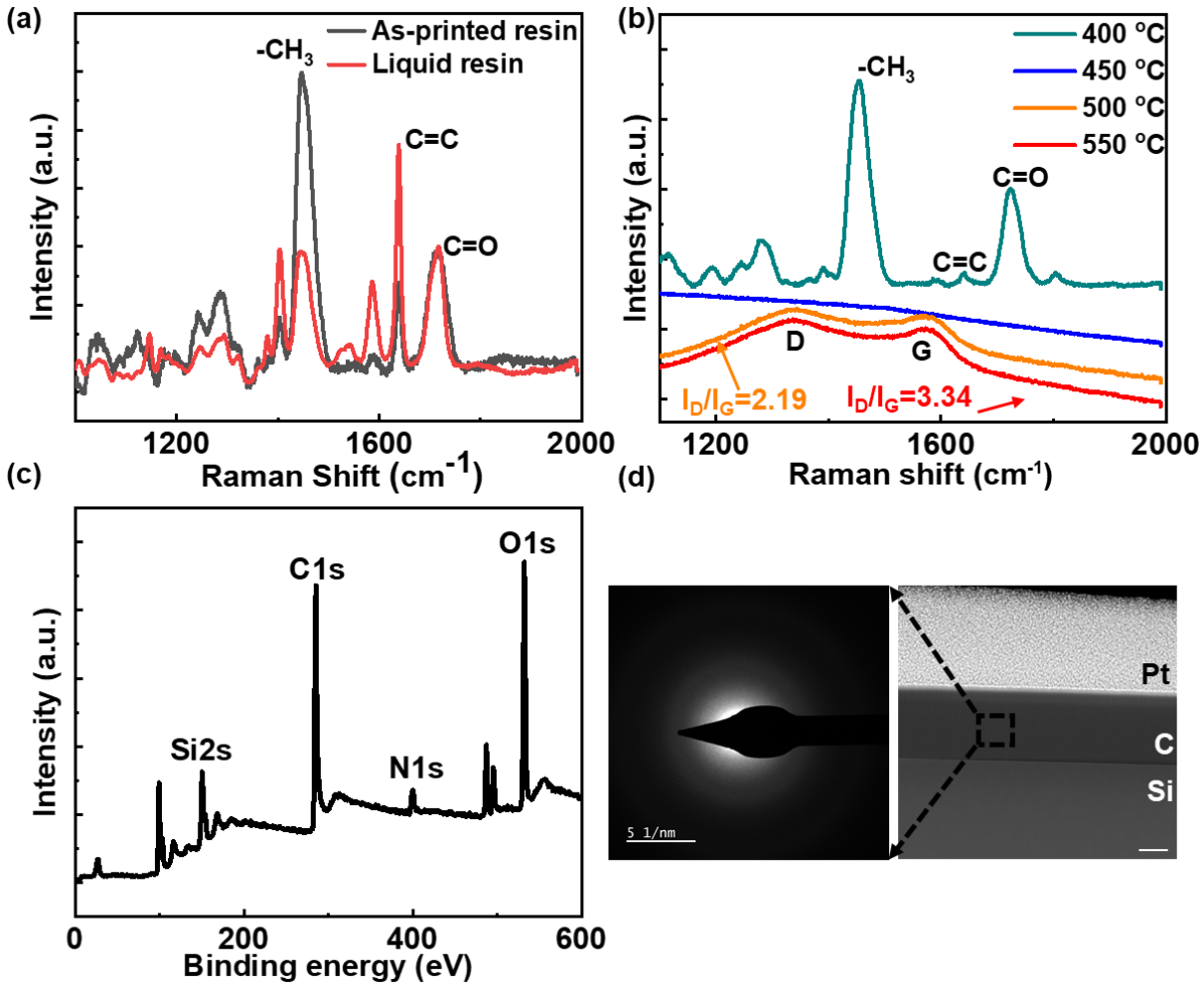

Figure 2. Evolution of chemical bonds and microstructure as a function of pyrolysis temperature. (a) Raman spectra collected from unpolymerized resin and as-printed structures respectively. (b) Raman spectra of samples pyrolyzed at different temperatures, with ramp rate and pyrolysis time fixed at 15 °C /min and 5 min respectively. (c) XPS survey spectra of resultant carbon material. Si and other metal signals are from contamination (d) SAED and HAADF image of resultant carbon. Scale bar: 100 nm.

The resultant carbon material was also characterized by X-ray photoelectron spectroscopy (XPS) and transmission electron microscopy (TEM), respectively, as shown in Figures 2c&d with XPS details provided in Figure S4. A significant amount of nitrogen and

[#]Authors contributed equally to this paper.

oxygen originating from monomer and crosslinked polymer remain inside the pyrolyzed products, which are also verified by the XPS C1s spectra provided in Figure S4, and the binding energy fitted at 284.8, 286, and 289 eV were assigned to carbon atoms in the C=C/C-C, C-N, and C=O bonds respectively. The diffuse ring observed by the TEM in the selected area diffraction mode indicates that the inner structure of the pyrolyzed carbon is amorphous with no crystallinity, which is very similar to the studies on SU-8 as the nucleation of long-chain carbon into nanocrystallites required much higher temperature.[37,38] In conclusion, there are three stages of compositional changes during pyrolysis as the temperature increases. The first stage is the evaporation of monomers which occurs at relatively low temperatures. At higher temperatures, bond cleavage leading to decomposition occurs and is followed by carbonization with a significant release of heteroatoms.

3.2 Volume shrinkage & change of mechanical property during pyrolysis

Along with changes in chemical composition, mechanical properties and shrinkage also are observed. To measure the shrinkage, the same foam structures (foam structures pyrolyzed from 400 to 550 °C with a constant ramp rate of 15 °C/min and held for 5 min at the pyrolysis temperature) mentioned in Section 3.1 were coated with chromium and characterized by scanning electron microscopy to measure the dimensions of pyrolyzed foams. The shrinkage ratio (S_v) is defined as:

$$S_v = \frac{D_0^3 - D_1^3}{D_0^3}$$

where D_0 is the diameter of the designed foam structures (500 μm), D_1 is the measured diameter of the foam structures from the SEM images. As can be seen in Figure 3a, the overall trend of the shrinkage as well as weight loss monotonically increases with the temperature increasing. In

[#]Authors contributed equally to this paper.

the range after ~375 °C, the volume shrinkage surpass weight loss, which may indicate that with the severe volume reduction, the density of the pyrolyzed material starts to increase in this range. Combined with the evolution of chemical composition, the main material loss, as well as shrinkage, occurs between the range of 300-400 °C and 450-550 °C, where monomer evaporation, decomposition, and release of heteroatoms are the dominant mechanisms. Along with macroscopic volume reduction, the printed line width also shrunk to 405 nm, and this dimension is nearly a factor of four beneath the two-photon diffraction limit ($\frac{\lambda}{\sqrt{2}*NA}$=1.84 μm) of the 2PP objective lens used, as shown in Figure S5. By further increasing the pyrolysis temperature to 600 °C, the printed line width shrunk to 399 nm, which correlates with the TGA curve where the material loss approaches saturation at high temperature, which is quite different from the reported pyrolysis of SU-8 that stabilized at ~80% mass loss after pyrolysis.[37,39] In addition to shrinkage, we also noticed that the surface morphology of the printed material also evolves during pyrolysis, as shown in Figures 3c-f. Nanoscale wrinkles were observed at low temperatures whereas after the release of heteroatoms, the surface become extremely smooth.

In anticipation of material hardening upon pyrolysis, we measured the Young's modulus using an atomic force microscopy (Bruker Corporation, Dimension Icon) with a Tap300A tip. To make sure that the structures are stable for indentation, solid cubes were printed with a laser power of 50 mW and a scan speed of 20 mm/s, and samples were subsequently pyrolyzed at different temperatures (315-475 °C). As shown in Figure 3b, with the possibility of further crosslinking and evaporation of monomers, the material hardens, indicating that densification is the dominant process in this stage.[40] However, with bond cleavage leading ot thermal decomposition, there is a significant deterioration of mechanical properties and the Young's modulus decreases from ~19.3 to ~8.2 GPa. Upon further increasing the pyrolysis temperature,

[#]Authors contributed equally to this paper.

the hydrogen and oxygen atoms are released from the structures, and carbon atoms start to hybridize and form glassy carbon, where the Young's modulus again increases. Compared with carbon material pyrolyzed from SU-8, the IP-Q pyrolyzed carbon material shows a lower Young's modulus.[39,41]

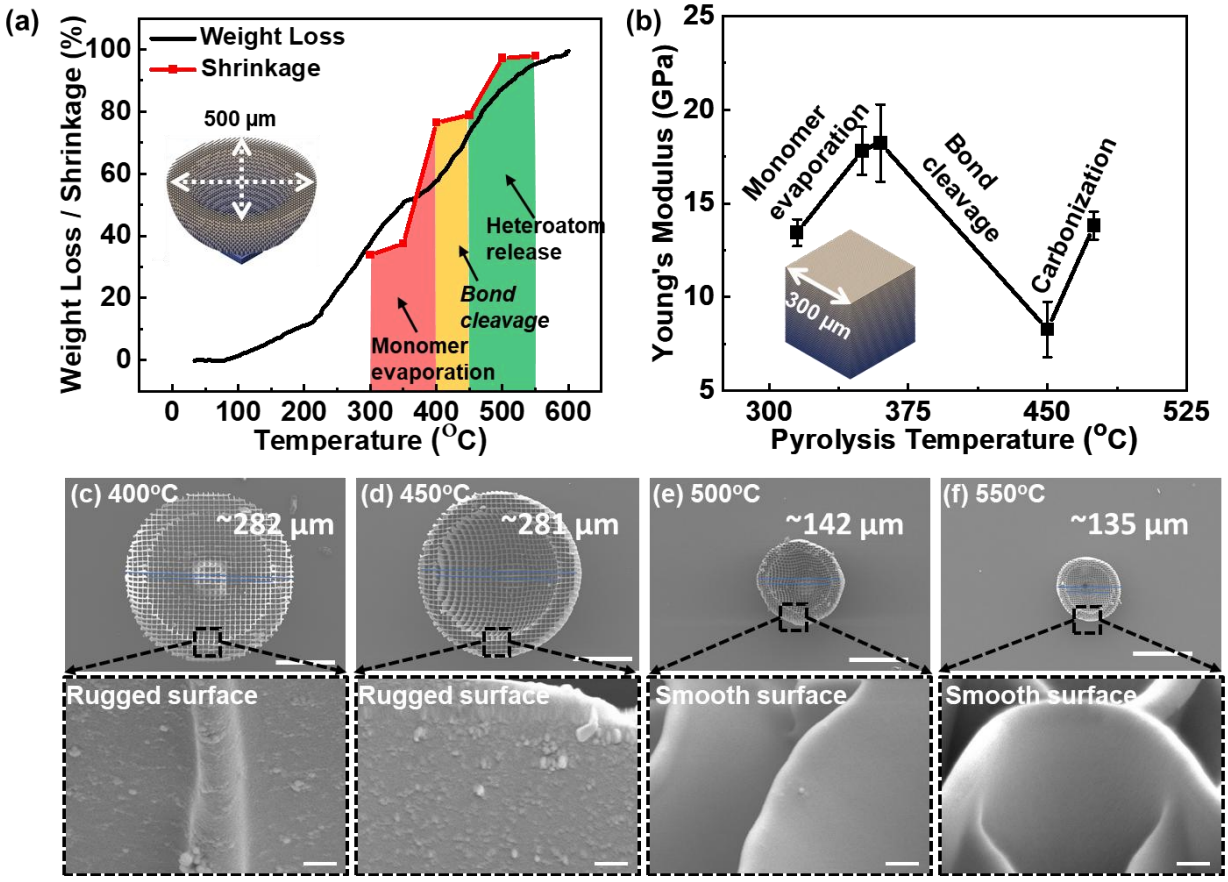

Figure 3. Evolution of shrinkage, mechanical properties, and surface morphologies during pyrolysis. (a) The overlapped graph of TGA analysis and measured shrinkage of the samples pyrolyzed at different temperatures, with ramp rate and pyrolysis time fixed at 15 °C/min and 5 min, respectively. (b) Measured Young's modulus collected from samples pyrolyzed at different temperatures, with the ramp rate and pyrolysis time fixed at 10 °C/min and 5 min, respectively. For each sample, five measurements were averaged for determination of the Young's modulus. (c) Representative SEM images for the measurements of shrinkage in (a) and zoomed-in SEM images of surface morphologies of each sample. Scale bars are: 100 µm and 500 nm respectively.

3.3 Evolution of surface roughness during pyrolysis

In addition to the shrinkage of printed features upon pyrolysis, we also observed a concomitant reduction in surface roughness. To begin with, the surface roughness of 2PP 3D structures

[#]Authors contributed equally to this paper.

originated from the fact that the 3D structures were printed line-by-line, followed by layer-by-layer. Based on this principle, smaller hatching and slicing distances are usually used to reduce surface roughness, as reported by others.[42,43] After pyrolysis, the hatching and slicing distances were reduced due to material loss and shrinkage as evident from laser scanning microscopy (LSM) images of printed shell structures shown in Figure 4. By setting the slicing distance at 2 μm, we printed 3 semi-shell structures with support structures so that they can shrink freely on the substrate and pyrolyzed two of them at 360 and 420 °C, respectively; and the remaining one remained un-pyrolyzed. After correcting the baseline and overlapping the profile image at the polar point, the LSM measurements show that the layer thickness (mainly determined by slicing distance) was reduced from 2.00 to 1.63 μm. Consequently, after subtracting a least-squares-fit spherical cap, the root mean square surface roughness Rq within the highlighted area in Figures 4b-d, is reduced from 4 to 2.7 μm upon pyrolysis at 420 °C. However, the shell structure significantly deformed into an oval shape upon pyrolysis at 420 °C, as shown in Figure 4a and the SEM images in Figure S6, which suggests that the shrinkage becomes anisotropic under this temperature. By further increasing the pyrolysis temperature above 500 °C, printed structures such as the 3D shell collapse into films due to severe material loss, as shown in Figure 4e. Moreover, optical observation shows no step features in the resultant glassy carbon films, which indicates the potential for fabrication of ultra-smooth carbon structures if the pyrolysis recipe is finely tuned such that 3D features survive through the carbonization process, as reported by Serles *et al*.[41]

4. Conclusions

In summary, Raman microscopy, XPS, nanoindentation, TEM, and SEM were used to investigate 2PP structures pyrolyzed under different conditions. Our results reveal the key

[#]Authors contributed equally to this paper.

physical and chemical processes that occur during pyrolysis, namely, monomer evaporation, chemical decomposition, and carbonization. We also identified how the Young's modulus evolves during pyrolysis with increasing temperature. First, the modulus increases due to monomer loss and crosslinking, then decreases due to bond cleavage upon chemical decomposition, and finally increases upon the formation of glassy carbon structures. Further analyses indicate that monomer evaporation and carbonization lead to material shrinkage and reduce surface roughness. Improving Young's modulus and surface finish are both desired for 2PP, and our results can be immediately applied to fabrication of laser fusion targets and C-MEMS.

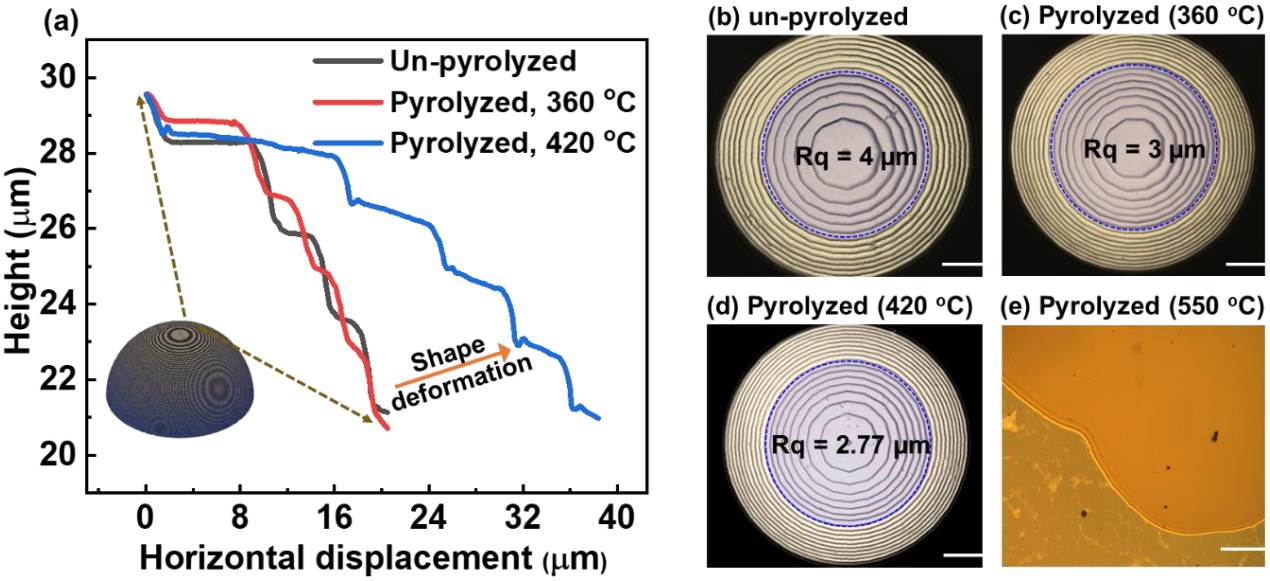

Figure 4. Improvement of surface smoothness with pyrolysis temperature. (a) the profile of pyrolyzed and un-pyrolyzed shell structures by setting slicing distance = 2 μm during printing. (b-e) The LSM and optical images of the polar region of pyrolyzed and un-pyrolyzed shells. Scale bar: 50 μm. For the pyrolyzed shell, the pyrolysis receipt is: ramp rate=10 ^{o}C/min, maximum temperature=360 and 420 ^{o}C respectively, hold 5 min at maximum temperature and cool down naturally in an argon atmosphere.

5. Conflict of Interest

The authors declare no conflict of interest.

[#]Authors contributed equally to this paper.

6. Acknowledgment.

The research was partially supported by the National Science Foundation (under Award CMMI 1826392) and Nebraska Center for Energy Sciences Research (NCESR), The research was performed in part in the Nebraska Nanoscale Facility: National Nanotechnology Coordinated Infrastructure and the Nebraska Center for Materials and Nanoscience (and/or NERCF), which are supported by the National Science Foundation under Award ECCS: 2025298, and the Nebraska Research Initiative.

Aofei Mao, Hibiki Mitsuboshi, and Maxime Trochon contributed equally to this work.

Reference.

1. Farsari, M. & Chichkov, B. N. Two-photon fabrication. *Nat. Photonics* **3**, 450–452 (2009).
2. Zhou, X., Hou, Y. & Lin, J. A review on the processing accuracy of two-photon polymerization. *AIP Adv.* **5**, 030701 (2015).
3. Liu, Y. *et al.* Deformation Behavior of Foam Laser Targets Fabricated by Two-Photon Polymerization. *Nanomater. Basel Switz.* **8**, (2018).
4. Campbell, J. H. *et al.* Three-dimensional printing and deformation behavior of low-density target structures by two-photon polymerization. in *Nanoengineering: Fabrication, Properties, Optics, and Devices XIV* (eds. Campo, E. M., Dobisz, E. A. & Eldada, L. A.) 66 (SPIE, 2017). doi:10.1117/12.2274193.
5. Mao, A. *et al.* Forming three-dimensional micro-objects using two-dimensional gradient printing. *Appl. Mater. Today* **28**, 101538 (2022).
6. Zhang, Y.-L. *et al.* Dual-3D Femtosecond Laser Nanofabrication Enables Dynamic Actuation. *ACS Nano* **13**, 4041–4048 (2019).

[#]Authors contributed equally to this paper.

7. Duc Nguyen, H. H. *et al.* Freeform three-dimensional embedded polymer waveguides enabled by external-diffusion assisted two-photon lithography. *Appl. Opt.* **55**, 1906 (2016).
8. Hernandez, D. L. G. *et al.* Laser 3D Printing of Inorganic Free-Form Micro-Optics. (2021) doi:10.20944/preprints202111.0136.v1.
9. Cardenas-Benitez, B. et al. Pyrolysis-induced shrinking of three-dimensional structures fabricated by two-photon polymerization: experiment and theoretical model. Microsyst Nanoeng 5, 1–13 (2019).
10. Tiwari, A. & Raj, B. *Materials and Failures in MEMS and NEMS*. (John Wiley & Sons, 2015).
11. Sharipova, M. I. *et al.* Effect of pyrolysis on microstructures made of various photoresists by two-photon polymerization: comparative study. *Opt. Mater. Express* **11**, 371–384 (2021).
12. Xiong, W. *et al.* Laser-Directed Assembly of Aligned Carbon Nanotubes in Three Dimensions for Multifunctional Device Fabrication. *Adv. Mater.* **28**, 2002–2009 (2016).
13. Hu, Q. *et al.* Additive manufacture of complex 3D Au-containing nanocomposites by simultaneous two-photon polymerisation and photoreduction. *Sci. Rep.* **7**, 17150 (2017).
14. Liu, Y. *et al.* Precise assembly and joining of silver nanowires in three dimensions for highly conductive composite structures. *Int. J. Extreme Manuf.* **1**, 025001 (2019).
15. Kotz, F. *et al.* Two-Photon Polymerization of Nanocomposites for the Fabrication of Transparent Fused Silica Glass Microstructures. *Adv. Mater.* **33**, 2006341 (2021).
16. Wang, W.-K. *et al.* Magnetic Nickel–Phosphorus/Polymer Composite and Remotely Driven Three-Dimensional Micromachine Fabricated by Nanoplating and Two-Photon Polymerization. *J. Phys. Chem. C* **115**, 11275–11281 (2011).
17. Suter, M. *et al.* Superparamagnetic microrobots: fabrication by two-photon polymerization

[#]Authors contributed equally to this paper.

and biocompatibility. *Biomed. Microdevices* **15**, 997–1003 (2013).

18. Formanek, F. *et al.* Three-dimensional fabrication of metallic nanostructures over large areas by two-photon polymerization. *Opt. Express* **14**, 800–809 (2006).
19. Xia, X. *et al.* Electrochemically reconfigurable architected materials. *Nature* **573**, 205–213 (2019).
20. Rys, J. *et al.* Fabrication and Deformation of Metallic Glass Micro-Lattices. *Adv. Eng. Mater.* **16**, 889–896 (2014).
21. Gross, A. J. & Bertoldi, K. Additive Manufacturing of Nanostructures That Are Delicate, Complex, and Smaller than Ever. *Small* **15**, 1902370 (2019).
22. Bauer, J., Schroer, A., Schwaiger, R. & Kraft, O. Approaching theoretical strength in glassy carbon nanolattices. *Nat. Mater.* **15**, 438–443 (2016).
23. Schueller, O. J. A., Brittain, S. T. & Whitesides, G. M. Fabrication of glassy carbon microstructures by pyrolysis of microfabricated polymeric precursors. *Adv. Mater.* **9**, 477–480 (1997).
24. Crook, C. *et al.* Plate-nanolattices at the theoretical limit of stiffness and strength. *Nat. Commun.* **11**, 1579 (2020).
25. Narita, K., Citrin, M. A., Yang, H., Xia, X. & Greer, J. R. 3D Architected Carbon Electrodes for Energy Storage. *Adv. Energy Mater.* **11**, 2002637 (2021).
26. Yang, C. *et al.* 3D-Printed Carbon Electrodes for Neurotransmitter Detection. *Angew. Chem. Int. Ed.* **57**, 14255–14259 (2018).
27. Zakhurdaeva, A. *et al.* Custom-Designed Glassy Carbon Tips for Atomic Force Microscopy. *Micromachines* **8**, 285 (2017).
28. Liu, Y. *et al.* Structural color three-dimensional printing by shrinking photonic crystals. *Nat.*

[#]Authors contributed equally to this paper.

Commun. **10**, 4340 (2019).

29. Zhao, Z. *et al.* Atomic Layer Deposition Inducing Integration of Co, N Codoped Carbon Sphere on 3D Foam with Hierarchically Porous Structures for Flexible Hydrogen Producing Device. *Adv. Funct. Mater.* **29**, 1906365 (2019).
30. Zhao, Z. *et al.* Atomic layer deposition-assisted fabrication of 3D Co-doped carbon framework for sensitive enzyme-free lactic acid sensor. *Chem. Eng. J.* **417**, 129285 (2021).
31. Kong, Y. *et al.* Integration of a Metal–Organic Framework Film with a Tubular Whispering-Gallery-Mode Microcavity for Effective CO_2 Sensing. *ACS Appl. Mater. Interfaces* **13**, 58104–58113 (2021).
32. Seniutinas, G. *et al.* Beyond 100 nm resolution in 3D laser lithography — Post processing solutions. *Microelectron. Eng.* **191**, 25–31 (2018).
33. Jang, J., Panusa, G., Boero, G. & Brugger, J. SU-8 cantilever with integrated pyrolyzed glass-like carbon piezoresistor. *Microsyst. Nanoeng.* **8**, 1–12 (2022).
34. Bernard, S. *et al.* XANES, Raman and XRD study of anthracene-based cokes and saccharose-based chars submitted to high-temperature pyrolysis. *Carbon* **48**, 2506–2516 (2010).
35. Keown, D. M., Li, X., Hayashi, J. & Li, C.-Z. Characterization of the Structural Features of Char from the Pyrolysis of Cane Trash Using Fourier Transform−Raman Spectroscopy. *Energy Fuels* **21**, 1816–1821 (2007).
36. Ferrari, A. C. & Robertson, J. Interpretation of Raman spectra of disordered and amorphous carbon. *Phys. Rev. B* **61**, 14095–14107 (2000).
37. Singh, A., Jayaram, J., Madou, M. & Akbar, S. Pyrolysis of Negative Photoresists to Fabricate Carbon Structures for Microelectromechanical Systems and Electrochemical

[#]Authors contributed equally to this paper.

Applications. *J. Electrochem. Soc.* **149**, E78 (2002).

38. Lim, Y., Heo, J.-I., Madou, M. & Shin, H. Monolithic carbon structures including suspended single nanowires and nanomeshes as a sensor platform. *Nanoscale Res. Lett.* **8**, 492 (2013).

39. Lee, J. A., Lee, S. W., Lee, K.-C., Park, S. I. & Lee, S. S. Fabrication and characterization of freestanding 3D carbon microstructures using multi-exposures and resist pyrolysis. *J. Micromechanics Microengineering* **18**, 035012 (2008).

40. Amza, C. G., Zapciu, A., Constantin, G., Baciu, F. & Vasile, M. I. Enhancing Mechanical Properties of Polymer 3D Printed Parts. *Polymers* **13**, 562 (2021).

41. Serles, P. *et al.* Mechanically robust pyrolyzed carbon produced by two photon polymerization. *Carbon* **201**, 161–169 (2023).

42. Liao, C., Anderson, W., Antaw, F. & Trau, M. Two-Photon Nanolithography of Tailored Hollow three-dimensional Microdevices for Biosystems. *ACS Omega* **4**, 1401–1409 (2019).

43. Takada, K., Sun, H.-B. & Kawata, S. Improved spatial resolution and surface roughness in photopolymerization-based laser nanowriting. *Appl. Phys. Lett.* **86**, 071122 (2005).

[#]Authors contributed equally to this paper.